Author Manuscript

Author Manuscript

Author Manuscript

Author Manuscript

HHS Public Access

Author manuscript

J Pharm Sci. Author manuscript; available in PMC 2018 August 15.

Published in final edited form as:

J Pharm Sci. 2018 March ; 107(3): 922–933. doi:10.1016/j.xphs.2017.10.042.

INJECTABLE HYDROGELS FOR LOCALIZED CHEMO- AND RADIO-THERAPY IN BRAIN TUMORS

Pilar de la Puente[1], **Nicole Fettig**[2], **Micah J. Luderer**[1], **Abbey Jin**[1,3], **Shruti Shah**[1], **Barbara Muz**[1], **Vaishali Kapoor**[1], **Sreekrishna M. Goddu**[1], **Noha Nabil Salama**[3,4], **Christina Tsien**[1,5], **Dinesh Thotala**[1,5], **Kooresh Shoghi**[2,5], **Buck Rogers**[1,5], and **Abdel Kareem Azab**[1,5,*]

[1]Department of Radiation Oncology, Washington University in Saint Louis School of Medicine

[2]Radiology and Biomedical Engineering Department, Preclinical PET/CT Imaging Facility, Washington University in Saint Louis School of Medicine

[3]Department of Pharmaceutical and Administrative Sciences, St. Louis College of Pharmacy, St. Louis, Missouri

[4]Department of Pharmaceutics and Industrial Pharmacy, Cairo University Faculty of Pharmacy, Cairo, Egypt

[5]Siteman Cancer Center, Washington University in Saint Louis School of Medicine

Abstract

Purpose: Overall survival of patients with newly diagnosed glioblastoma (GBM) remains dismal at 16 months with state-of-the-art treatment that includes surgical resection, radiation and chemotherapy. GBM tumors are highly heterogeneous and mechanisms for overcoming tumor resistance have not yet fully been elucidated. An injectable chitosan hydrogel capable of releasing chemotherapy (Temozolomide, TMZ) while retaining radioactive isotopes agents (Iodine, ^{131}I) was used as a vehicle for localized radiation and chemotherapy, within the surgical cavity.

Methods: Release from hydrogels loaded with TMZ or ^{131}I was characterized in vitro and in vivo and their efficacy on tumor progression and survival on GBM tumors was also measured.

Results: The in vitro release of ^{131}I was negligible over 42days, while the TMZ was completely released over the first 48 hours. ^{131}I was completely retained in the tumor bed with negligible distribution in other tissues and that when delivered locally the chemotherapy accumulated in the

*Corresponding Author: Abdel Kareem Azab, Ph.D., B. Pharm., Department of Radiation Oncology, Cancer Biology Division, Washington University in Saint Louis School of Medicine, 4511 Forest Park Ave., Room 3103, St. Louis, MO 63108, Office (314) 362-9254; Fax (314) 362-9790, kareem.azab@wustl.edu.

AUTHORSHIP

Contribution: P.P. performed experiments, designed the study, analyzed, interpreted the data and wrote the manuscript; N.F., M.L., and A.J, S.S., performed research and analyzed data; B.M., V.K., M.G., D.T., K.S., B.R., N.N.S., analyzed and interpreted data; C.T., provided clinical rationale and edited the manuscript; A.K.A., designed and supervised the study, interpreted the data and edited the manuscript. All authors reviewed and approved the manuscript.

CONFLICT OF INTERESTS

Dr. Azab receives research support from Verastem, Selexys, Karyopharm, Cell Works, Cleave Bioscience, Glycomimetics, Abbvie and Vasculox; and is the founder and owner of Targeted Therapeutics LLC and Cellatrix LLC, however there has been no contribution of the aforementioned entities to the current study. Dr. de la Puente is a co-founder of Cellatrix LLC, however, there has been no contribution to the current study. Dr. de la Puente and Dr. Azab have a provisional patent application on the technology described in this manuscript. Other authors state no conflicts of interest.

Author Manuscript Author Manuscript Author Manuscript Author Manuscript

tumor at 10-fold higher concentrations compared to when delivered systemically. We found that the tumors were significantly decreased and survival was improved in both treatments groups compared to the control group.

Conclusions: Novel injectable chemo-radio-hydrogel implants may potentially improve the local control and overall outcome of aggressive, poor prognosis brain tumors.

Graphical abstract

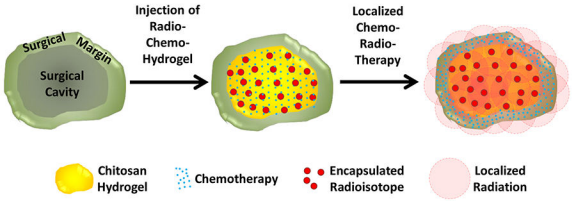

Keywords

Glioblastoma; localized chemotherapy; localized radiotherapy; hydrogels; injectable

INTRODUCTION

Overall survival of patients with newly diagnosed glioblastoma (GBM) remains dismal at 16 months with state-of-the-art treatment that includes surgical resection, external beam radiation and chemotherapy. The majority of GBM tumors recur locally despite targeting the tumor as well as its surrounding margin of the normal brain without distant failure. Necessary radiotherapy (RT) doses required for improved local tumor control exceeds normal brain tissue tolerance and increased RT necrosis. Additionally, the blood brain barrier has stymied development of effective radio-sensitizers and systemic chemotherapies. GBM tumors are highly heterogeneous and mechanisms for overcoming tumor resistance have not yet fully been elucidated. Alternative therapeutic strategies for the treatment of GBM are therefore clearly warranted.

Localized radiotherapy offers a potential strategy for improved tumor targeting precision while sparing normal tissues [1,2]. Traditional placement of radioactive brachytherapy seeds in the surgical cavity have proved difficult in achieving the desired homogeneity of RT dose distributed to margins due to irregularities in cavity shape. More recent efforts have used balloons and a catheter to deliver a radioactive source (Gliasite® Radiation Therapy System)[3]. Implantation of iridium-192 and iodine-125 seeds and the balloon-based brachytherapy have shown activity in primary malignant gliomas [4-8]. However, randomized studies using interstitial radiation boosts have not demonstrated an improved outcome compared to standard therapy [9]. The use of an injectable biodegradable hydrogel, loaded with chemo- and radio-therapy, with the ability to fill the post resection cavity entirely regardless of its shape and degree of deformity should facilitate greater homogeneity of doses and may lead to improved outcomes.

Author Manuscript Author Manuscript Author Manuscript Author Manuscript

In lieu of intravenous chemotherapy, treatment plans are increasingly turning to localized methods of delivery. Biodegradable carmustine wafers (Gliadel) placed in the surgical cavity after removal of GBM have gained increased acceptance. Gliadel wafers loaded with carmustine were shown to significantly increase median survival versus placebo wafers in the treatment of GBM, with a diffusion capacity of about 2mm [10,11]. The wafers are solid and thus do not entirely fill the post-resection cavity. This can contribute to non-homogeneous distribution of chemotherapy.

The goal of the present study was to test the feasibility of a novel delivery system for local chemo-radio-therapy treatment of GBM. A biodegradable injectable chitosan hydrogel capable of releasing chemotherapy while retaining radioactive isotopes agents was used as a vehicle for localized radiation and chemotherapy within the surgical cavity. The study involved exploring new approaches of previous efforts at using brachytherapy techniques to treat central nervous system lesions, and development of an efficient and highly controllable means of delivering localized chemotherapy to address and enhance the chemotherapeutic effectiveness across the blood brain barrier.

MATERIALS AND METHODS

Materials & Reagents

Unless stated otherwise, all materials were purchased from Sigma (St. Louis, MO, USA). Chitosan (low molecular weight, 50,000-190,000 Da based on viscosity, Sigma Product #448869), acetic acid 99.7%, and glutaraldehyde (GA) solution 25% were used for the preparation of the chitosan hydrogels. Alginic acid sodium salt from brown algae (low viscosity 4-12cP), sodium bicarbonate, and calcium chloride were used for the elaboration of microparticles. Fluorescein isothiocyanate (FITC) and Bovine Serum Albumin (BSA)-FITC (BSA-FITC) were purchased from MP Biomedicals (Solon, OH, USA) and used for evaluation of *in vitro* release. Volumex (Iodine-131 (^{131}I) Human Serum Albumin (HSA)) was purchased from Daxor Corporation (New York, NY, USA). Doxorubicin and temozolomide (TMZ) were purchased from Selleckchem (Houston, Tx, USA). Corning Matrigel Basement Membrane Matrix Growth Factor Reduced (Corning, New York, NY, USA) was prepared following manufacturer instructions for *in vivo* implantation.

Cells

Glioma (D54 and D54-GFP-luc) cell lines were a kind gift from Dr. Dinesh Thotala (Department of Radiation Oncology, Cancer Biology Division, Washington University in Saint Louis School of Medicine). All cell lines were cultured in DMEM with F-12 Nutrient Mixture in a 1:1 ratio supplemented with 10% fetal bovine serum (FBS, Gibco, Life Technologies, Grand Island, NY), 2 mmol/L L-glutamine, 100 U/mL Penicillin and 100 μg/mL Streptomycin (CellGro, Mediatech, Manassas, VA). Before plating, cells were washed with phosphate-buffered saline (PBS, Corning CellGro, Mediatech, Manassas, VA), trypsinized with 0.05% Trypsin-EDTA 1x (Gibco, Life Technologies, Grand Island, NY), spun for 5 minutes (1000 RPM) and resuspended in fresh DMEM:F12 media.

Author Manuscript Author Manuscript Author Manuscript Author Manuscript

Animals and tumor development

Nude (Hsd: Athymic Nude-Foxn1nu) 5-6 week old female mice (Harlan) were used for animal studies. Animal procedures were approved by the Institutional Animal Care and Use Committee (IACUC) at Washington University School of Medicine in St. Louis. Mice were anesthetized with ketamine/xylazine and injected subcutaneously with 150 μl matrigel at a final concentration of 6 mg/ml containing 1 million D54-GFP-luc cells into the right flank, as previously described [12]. After 10-14 days, tumors were palpable, and mice were stratified for treatments.

Preparation of Chitosan hydrogels

Chitosan hydrogels were produced based on previously described methods [13]with the following modifications. Briefly, chitosan (1 g) was dissolved in 100 ml of 0.1 M acetic acid. While chitosan solution was being stirred, different GA solution concentrations (0.1-5% w/v in water) were added. A hydrogel was immediately formed, and stirring was stopped thereafter. Chitosan hydrogels were allowed to stabilize for 4 hours before characterization.

Crosslinking and shear-stress characterization of Chitosan hydrogels

Crosslinking was measured by quantification of absorbance uptake of hydrogels and Fourier Transform Infrared Spectroscopy (FTIR). Representative pictures of the chitosan hydrogels were taken 4 h after crosslinking to show their appearance. Then, crosslinked chitosan hydrogels' absorbance at 360 nm (SpectraMax i3, Molecular Devices, Sunnyvale CA) were determined. FTIR was used to characterize the presence of specific chemical groups in the materials. Chitosan hydrogels crosslinked with GA were analyzed by FTIR using Transmittance Mode. FTIR spectra were obtained in the range of wavenumber from 4000 to 500 cm− 1 during 32 scans (NEXUS 470 FT-IR, SMART PERFORMER, Thermo Nicolet, USA). The FTIR spectra were normalized by reducing the background noise of non-crosslinked chitosan hydrogels and major vibration bands were associated with chemical groups.

In addition, chitosan hydrogels from varying GA concentrations were characterized by one of three appearance levels: liquid, semi-solid or solid. The injectability of chitosan hydrogels was analyzed by using shear-stress characterization. The shear-stress technique analyzed 4ml of chitosan hydrogel contained in a 5ml syringe. The syringe was loaded with 4ml of pre-crosslinked hydrogels using a pipette (liquid hydrogels), a spatula (semi-solid hydrogels) or small pieces by hand (solid hydrogels). A constant force was applied to the top of the syringe and dispersing time of various amounts of hydrogel (1/4, 2/4, 3/4, and full volume) was measured. The results (amount of hydrogel dispersed vs time*force) showed the shear-stress properties of the crosslinked chitosan hydrogels. A qualitative determinacion of injectability was performed by 10 properly trained participants following the previously described method [14]. The participants were asked to evaluate the injectability of 4ml aliquots of each formulation in a syringe by rating injection difficulty and the formulation flow through the syringe, using an arbitrary score from 1 to 4. In particular, the arbitrary score for both parameters was defined as following:

Author Manuscript Author Manuscript Author Manuscript Author Manuscript

Score 1 = injection difficulty: not possible; flow: no flow or drop wise;

Score 2 = injection difficulty: high; flow: initially drop wise, then continuous;

Score 3 = injection difficulty: medium; flow: continuous;

Score 4 = injection difficulty: low; flow: too fast.

Injectability for a specific formulation was considered acceptable when the total score was 30±2, meaning most of the volunteers were able to inject the tested formulation with medium injection difficulty obtaining steady flow.

We further characterized the viscosity of chitosan hydrogels. First, the viscosity profile of chitosan hydrogels from varying GA concentrations (0 – 0.6%) was carried out by Brookfield Digital Viscometer (Model DV-E, Spindle LV3, spindle multiplier constant 128). The chitosan hydrogels were taken 4 h after crosslinking in scintillation vials and measured the fluid's resistance to flow.

After viscosity was measured, the swelling properties of chitosan crosslinked with 0.4% GA were evaluated. Pre-weighed hydrogel was immersed in excess of swelling medium (double distilled water, DDW). At various time intervals, the swelling medium was removed and hydrogel weighed after excessive solution of the surface was blotted. Results were calculated according to the following equation: $Q = (Ws - Wd) / Wd$. Here, Q is the swelling ratio, Ws is the weigth in the swollen state and Wd is the weigth in the dried state.

Preparation of Alginate microparticles

Alginate microparticles were obtained by inducing the crosslinking of an alginate solution with calcium chloride. When sodium alginate solution is added into a solution of calcium ions, the calcium ions displace the sodium ions in the alginate polymer. Various alginate concentrations (10-100 mg/ml) were dissolved in 0.1 M sodium bicarbonate by first grinding the alginate in a mortar and followed by mixing with a magnetic stirrer. Once dissolved, this alginate solution was added drop-wise with a 30G needle to a 0.1 M calcium solution without stirring. The alginate microparticles were washed three times with DDW.

Alginate microparticles size characterization

The morphological examination of the microparticles was performed by an optical microscope (Olympus ix70 inverted microscope). The size of alginate microparticles was measured from microscopic images (QICAM Fast 1394 Digital Camera) by using image analysis software (Image J, NIH, Bethesda, MD).

In vitro release studies of chitosan hydrogels loaded with alginate microparticles

The chitosan hydrogels with the best injectability properties (chitosan crosslinked with 0.4% GA) were analyzed naïve or loaded with the alginate microparticles that displayed the best encapsulation efficiency (Alginate 75 mg/ml). The *in vitro* release studies were performed by using FITC alone or linked to a large-size molecule such as BSA to detect the efficacy in both encapsulation settings (small and large-size molecules, respectively). BSA-FITC or

Author Manuscript Author Manuscript Author Manuscript Author Manuscript

FITC were loaded in alginate solution either by being dropped into calcium chloride to make microparticles and by direct incorporation into the chitosan hydrogel. Finally, the chitosan hydrogels (chitosan hydrogels with FITC directly dispersed, Ct-FITC; chitosan hydrogels with BSA-FITC directly dispersed, Ct-BSA-FITC; and chitosan hydrogels with BSA-FITC incorporated in alginate microparticles dispersed in the hydrogel, Ct-mAlg-BSA-FITC) were included in PBS (pH 7.4) at 4°C and were shaken in a light protected environment for 42 days. BSA-FITC and FITC were added to the PBS solution that contains chitosan naïve hydrogels as total release control, and also chitosan naïve hydrogels were included in PBS as blank. The PBS solution with the chitosan hydrogels was sampled and the samples were analyzed by fluorescence reader (BSA-FITC and FITC) at 485/516 nm at different time points for long-term release. The % release (%R) was calculated as follows: %R = (Ct − Blank) / (Total − Blank) *100.

Radioactive encapsulation efficiency and leakage in alginate microparticles

Volumex (^{131}I-HSA, 1.25 μCi) was mixed with 200 μl of 75 mg/ml alginate solution to make microparticles. Radioactive alginate microparticles (mAlg-^{131}I-HSA) were washed with DDW, and original supernatant, as well as the wash, were used for determination of encapsulation efficiency. The same amount of Volumex was used in DDW as a positive control. Radioactivity in the samples was determined using a Packard II gamma counter (PerkinElmer, Waltham, MA). The radioactivity encapsulation efficiency (rEE) was calculated as follows: %rEE = 100 − ([(mAlg-^{131}I-HSA$_{cpm}$)/Total$_{cpm}$]*100). Radioactive alginate microparticles contained approx. 1 μCi based on rEE and they were added to chitosan hydrogel (Ct-mAlg-^{131}I-HSA), which was included in PBS (pH 7.4) at room temperature and shaken in a light protected environment for 42 days. Samples from the PBS solution that surrounds the chitosan hydrogels at different time points for long-term release were analyzed for radioactivity using the gamma counter and leakage was calculated based on a decay-corrected standard dose (Volumex ^{131}I half-life 8 days). % Radioactivity Leakage (RL) was calculated as follows: %RL = [(Ct-mAlg-^{131}I-HSA$_{cpm}$ − Blank$_{cpm}$) / (decay-corrected Total − Blank$_{cpm}$)] *100.

Chemotherapy release from chitosan hydrogels

TMZ is a chemotherapeutic drug detectable by UV absorbance. TMZ calibration curve from 0 – 250 μg/ml was measured by a spectrophotometer at 325 nm. A final concentration of 250 μg/ml TMZ was incorporated in the previously described injectable chitosan hydrogels. The hydrogels were disperded in PBS (pH 7.4) at 4°C and were light protected and shaken for 48 h. TMZ was added to the PBS solution that contains chitosan naïve hydrogels as total, and also chitosan naïve hydrogels were included in PBS as blank. TMZ release into the PBS solution from the chitosan hydrogels was analyzed by spectrophotometer at 325 nm at various time points for 48 h. The percent release was calculated as previously shown for FITC and BSA-FITC.

Cell Survival Assay to chemotherapy

D54 cells were cultured with free-TMZ or equivalent chitosan hydrogels with TMZ directly dispersed (TMZ-Ct) added to the cells apically (0 – 100 μM) for 24h. The cells were detached by trypsinization and resuspended in fresh DMEM:F12 media. Cell viability was

Author Manuscript Author Manuscript Author Manuscript Author Manuscript

assessed using cell viability exclusion method with Vi-Cell cell counter (Beckman Coulter, Brea, CA).

In vivo radioactivity bio-distribution study

After tumors were palpable, 6 nude mice were injected with 200 μl chitosan hydrogel loaded with radioactive alginate microparticles (mAlg-^{131}I-HSA, 2 μCi/mice) at the tumor site. After 3 and 7 days, the mice were anesthetized, blood samples were collected, and tumors and distant organs (lung, liver, spleen, kidney, bladder, muscle, heart, and brain) were resected. Tissue samples were placed in a gamma counter (Beckman Gamma 8000) to measure radioactivity.

In vivo chemotherapy bio-distribution study

After tumors were palpable, 6 nude mice were assigned to receive either systemic i.v doxorubicin treatment (5mg/kg) (n=3) or an injection of 200 μl chitosan hydrogel loaded with equivalent doxorubicin concentration on top of the tumor (n=3). After 18 h, the mice were anesthetized, blood samples were collected, and tumors and distant organs (lung, liver, spleen, kidney, muscle, heart, and brain) were resected. Cells from blood samples were isolated using 1× red blood cell lysis buffer according to the manufacturer's protocol (BioLegend, San Diego, CA). The tissues were homogenized (Omni Tissue Homogenizer TH, Kennesaw, GA) in PBS, filtered, and diluted for flow cytometry analysis. Doxorubicin cellular uptake was determined by the mean fluorescence intensity (MFI) of doxorubicin (PE signal).

Survival and tumor progression study using mouse model

After tumors were palpable, 30 mice were imaged with bioluminescence imaging and then stratified into three groups of ten mice each. Mice were treated with localized TMZ-hydrogels containing an equivalent unique localized dose to systemic TMZ treated (5 days of 100mg/kg) (total dose of 10mg) [15] or hydrogels loaded with radioactive alginate microparticles ^{131}I. Radiation absorbed dose to the tumor was computed using the Medical Internal Radiation Dosimetry (MIRD) formalism assuming a spherical geometry. A 4 mm thick shell of ^{131}I labeled radioactive gel surrounds a 2 mm diameter tumor. The resulting 10 mm diameter unit density (1 g/cc) sphere is sub-divided into 5-concentric spheres and uniform activity distribution was assumed for the gel (outer 4 shells) while considering zero activity in the tumor (central sphere). Geometric factor approach was used to compute absorbed fractions and S-values to the central tumor from ^{131}I uniformly distributed in individual outer shells using the formalism proposed in Howell et al [16]. Dose to the tumor was computed from charged particle and photon emissions from ^{131}I. The computation assumes complete decay of radioactivity without any biological clearance. It was estimated that 120 μCi of ^{131}I is needed in the gel to deliver 4 Gy to the tumor. Mice weight and tumor growth (measured by bioluminescence imaging (BLI)) were recorded once a week. Survival of mice was monitored every day by the investigator.

Author Manuscript Author Manuscript Author Manuscript Author Manuscript

Statistical analysis

Measurements were made in triplicate for each group. The *in vitro* data were expressed as means ± standard deviation. Results were analyzed using student *t*-test for statistical significance and were considered significantly different for *p* value less than 0.05. The *in vivo* data were analyzed using student *t*-test or ANOVA for statistical significance, and results are depicted as mean ± S.E.M. Variation within each group was equally variant and similar between the groups that were statistically compared. Values were considered significantly different for *p* value less than 0.05.

RESULTS

Crosslinking and shear-stress characterization of chitosan hydrogels

The chemical crosslinking of chitosan with GA occurs through the nucleophilic attack of the amine group of the chitosan to the positively charged aldehyde group of GA forming an imine group in the crosslinked chitosan hydrogels (Figure 1A). Increasing the concentration of glutaraldehyde produced more extensive chitosan crosslinking resulting in more viscous hydrogels (Figure 1Bi). The quantification of crosslinking was performed based on the absorbance of the hydrogels at 360 nm. The reaction between chitosan and glutaraldehyde, results in an imine functional group (C=N). This type of chemical bond is historically known to have higher UV-VIS absorption than its starting functional groups, which allows the detection of the progression of the reaction by detection of the UV-Vis absorption, and have been used extensively for multiple biochemical applications, such as to detect conjugation to polymers (specifically chitosan) [17] and specific detection of imines [18]. Similarly, the shear-stress properties of chitosan hydrogels increased by increasing the concentration of glutaraldehyde. We identified three different types of crosslinking products: the hydrogels resulting from crosslinking with low amounts (0.1% and 0.2%) glutaraldehyde had very low absorbance similar to the non-crosslinked chitosan solution (0%). On the other hand, hydrogels resulting from high (1–5%) glutaraldehyde concentrations displayed the highest absorbance values (10-20 fold non-crosslinked chitosan solution). Finally, crosslinking with moderate glutaraldehyde concentrations (0.3–0.6%) resulted in intermediate absorbance (3–5 fold non-crosslinked chitosan solution) (Figure 1Bii).

FTIR spectra of crosslinked chitosan hydrogels with increasing glutaraldehyde concentrations is shown in Figure 1C. Increasing glutaraldehyde concentrations showed a different FTIR profile, with the presence of more intense vibrational bands at 1650 - 1550 cm^{-1} attributed to the imine functional group (C=N) revealing that chitosan is crosslinking with glutaraldehyde. In addition, the broad band from 3000 cm^{-1} to 3500 cm^{-1} is attributed to the stretching vibration of O-H and N-H of chitosan and the bands between the region 3200 cm^{-1} to 3400 cm^{-1} show the hydrogen bonded of O-H groups [1920].

Figure 2Ai shows the device used for shear-stress characterization following the proposed method by Ritschel to measure injectability by determining the time required to smoothly inject a solution under the specified pressure for a given syringe-needle system [21]. Figure 2Aii shows the better shear-stress profile of moderate concentrations of glutaraldehyde. Liquid hydrogels (0.1% and 0.2% glutaraldehyde) showed linear profile with rapid hydrogel

Author Manuscript Author Manuscript Author Manuscript Author Manuscript

dispersion. Solid hydrogels (0.6–5% glutaraldehyde) did not disperse due to their solid consistency and hence were not injectable or the consistency hampered injectability. Finally, semi-solid hydrogels (0.3–0.5%) showed linear profile with good injectability characteristics. All subjects tested were able to inject chitosan crosslinked with 0.4% Glutaraldehyde with a score of 3, meaning they were able to inject the tested formulation with medium difficulty obtaining steady flow (Table 1). Video 1 shows chitosan crosslinked with 0.2% GA, which is a liquid hydrogel with a score of 4 (low injection difficulty and rapid flow). Video 2 represents a semi-solid chitosan crosslinked (0.4% GA) hydrogel with score of 3 (medium injection difficulty and continuous flow), video 3 of chitosan crosslinked with 0.5% GA shows a semi-solid hydrogel with scoring of 2 (high injection difficulty and intermediate flow). Finally, in video 4 chitosan crosslinked with 1% GA is a solid hydrogel with score of 1 (not possible injection and no flow). Therefore, chitosan crosslinked with 0.4% GA (Figure 2Aiii) was selected for further experiments based on its linear shear-stress properties for injectability, for forming a hydrogel (not liquid and not solid) matrix, and in terms of the difficulty of injection and the formulation flow through the syringe.

Chitosan crosslinked hydrogels as shown in Figure 2B had viscosity range from 0.198 ± 0.008 Pa.s at 0% GA to 1967 ± 35.50 Pa.s at 0.6%, where the viscosity increased exponentially with increasing GA concentrations. The hydrogel used in further studies which had a final GA concentration of 0.4% had a viscosity of 1155.33 ± 169.02 Pa.s. Exactly, it appears to be a turning point in the viscosity around 0.4% GA, showing a transitional point of GA concentration where more solid hydrogels are formed. We further studied the swelling properties of chitosan hydrogels crosslinked with 0.4% GA in DDW. When the hydrogels were placed in pure water, the maximum osmotic pressure develops and hence the maximum swelling is achieved. Figure 2C shows chitosan hydrogels swelled fast during the first 8 h, until the equilibrium swelling ratio was achieved after this time.

Alginate microparticles size characterization

The ionic crosslinking of alginate with calcium ions (Ca^{2+}) occurs through the interaction of the divalent calcium cations with the carboxylic acid groups of two alginate chains forming an egg-box structure in the crosslinked alginate microparticles (Figure 3A)[22]. Microparticles immediately form when alginate is added drop-wise to a calcium solution. Increasing the concentration of alginate (up to a maximum of 75 mg/ml) produced smaller and spherical microparticles. Figure 3B shows the morphology of alginate particles crosslinked with $CaCl_2$ 0.1 M using different alginate concentrations. Microparticles resulting from low-medium alginate concentrations (10–75 mg/ml) possessed a spherical shape with a visible encapsulating shell. However, at high alginate concentration (100 mg/ml), the spherical shape and the shell were lost; no further analyses were realized for this alginate concentration. As shown in Figure 3C, increasing the concentration of alginate produced smaller microparticles, in which, 75 mg/ml alginate solution produced the smallest size 462.16 ± 62.09 μm. The alginate (75 mg/ml) crosslinked with $CaCl_2$ 0.1 M was selected for further experiments based on morphology and size.

Author Manuscript Author Manuscript Author Manuscript Author Manuscript

Release and leakage characterization of chitosan hydrogels and alginate microparticles *in vitro*

The release of small and large-size molecules was analyzed in naïve or microparticles-loaded chitosan hydrogels. Figure 4A shows that small molecule (FITC), when dispersed into the hydrogel directly (Ct-FITC), was released relatively fast from the hydrogel (at 14 days 100 ± 0.76 was released). However, when conjugated to a large molecule, BSA, and then dispersed in the chitosan hydrogel (Ct-BSA-FITC), the release significantly slowed down (at 42 days 49.53 ± 1.30% was released, $p<0.05$). On the other hand, when BSA-FITC was first encapsulated in alginate microparticles and then dispersed in the hydrogels (Ct-mAlg-BSA-FITC) the release was dramatically slowed down to less than 2% release in 42 days ($p<0.05$). These results emphasized that we could control the release of different substances from the hydrogel formulation based on size and encapsulation, a property which will be used to release chemotherapy and retain radiotherapy.

Then, we demonstrated that radioactivity could be loaded efficiently and retained in the hydrogel for long periods. First, Volumex (^{131}I-HSA) was encapsulated within the alginate microparticles with high encapsulation efficiency (90.12 ± 5.04%). The radioactive alginate microparticles (mAlg-^{131}I-HSA) were then incorporated within the chitosan hydrogels (Ct-mAlg-^{131}I-HSA), and the release of radioactivity from the hydrogel was measured, and found to be very low (less than 1%) after 42 days (Figure 4B).

Furthermore, we showed that the chemotherapeutic agent TMZ can be released from the hydrogel. TMZ was directly dispersed in the chitosan hydrogels (Ct-TMZ), and the release of TMZ out of chitosan hydrogels was measured. We found that TMZ was efficiently released from chitosan hydrogels within 48 h (Figure 4C). In the first 2 h, 50% of the drug was rapidly released, by 8 h reached almost 80%, and was fully released from the hydrogels after about 2 days. Finally, the effect of free-TMZ or Ct-TMZ hydrogels on D54 cell survival at different doses was tested *in vitro*. Free-TMZ and Ct-TMZ hydrogels were equally effective on cell survival at the different doses tested (Figure 4D), which indicates that the release of TMZ from chitosan hydrogels does not affect its potency.

In vivo radioactivity and chemotherapy bio-distribution

The strategy for localized chemo-radiotherapy of tumors relied on injection of the chitosan hydrogel into the tumor bed allowing localized release of chemotherapy while retaining the radiotherapy within the hydrogel to promote the local effect of the radiation and preventing systemic effects of the radiation. To confirm this strategy, we tested first the biodistribution of radioactivity and chemotherapy in tumor-bearing mice after implantation of the radio- or chemo-loaded chitosan hydrogels *in vivo* (Figure 5A). After implantation of radioactive hydrogel (Ct-mAlg-^{131}I-HSA), the bio-distribution of radioactivity was analyzed at days 3 and 7. We found that close to 99.96% of the radioactivity was localized in the tumor bed at both times point (Figure 5B), which reflects the efficacy of the radioactive microencapsulation in alginate microparticles and incorporation into chitosan hydrogels.

Next, we confirmed the local release of chemotherapy from the hydrogel into the tumor bed. Chemotherapy was directly dispersed in the chitosan hydrogel and implanted in the tumor

Author Manuscript Author Manuscript Author Manuscript Author Manuscript

bed and the biodistribution of the chemotherapeutic agent was measured. We found that the concentration of chemotherapeutic agent in the tumor was 10-fold higher than any other organ following the local delivery using the chitosan hydrogels (Figure 5C). To further demonstrate the superiority of the local delivery, the same dose of the chemotherapeutic agent applied locally was injected intravenously (i.v.), and analyzed its distribution after the systemic delivery. The biodistribution of the chemotherapeutic agent to the tumor was so limited compared to most other organs with the liver showing the highest drug amounts.

In vivo tumor progression and survival

Next, we examined the effect of localized chemotherapy and radiotherapy on tumor progression in mice with established tumors; treatment was initiated after a tumor progression signal was detected by BLI (around 3 weeks after injection of GBM cells). BLI images showed a decreased tumor size following localized treatments arms compared to control group (Figure 6A) at day 27 post-implantation. Tumor size was significantly lower in chemotherapy- ($p<0.03$) and radiotherapy-localized groups ($p<0.02$) compared to control (Figure 6B). The survival of control group was low, where all mice died around 29 days after starting the treatment. Treatment with localized chemotherapy or radiotherapy significantly prolonged mice survival in which 100% ($p<0.001$) and 80% ($p<0.001$) were still alive 35 days after treatment, respectively (Figure 6C).

DISCUSSION

GBM is the most common primary brain tumor in adults and continues to remain a devastating diagnosis [23]. The vast majority of GBM tumors recur [24], and almost always within the two-centimeter margin of tumor-brain interface [25,26]. The current standard of care includes surgical resection, radiotherapy, and chemotherapy [27,28]. Several localized treatment approaches have previously been tested including radioactive seeds, radioactive inflatable balloons, and biodegradable chemotherapy-loaded wafers. These approaches have not shown improvement in clinical outcomes in randomized studies, though retrospective studies have revealed modest improvements. Possible causes for concern focused on the homogeneity of the therapeutic dose to the surgical cavity plus the additional targeted margin leading to radionecrosis in regions receiving too much dose and recurrence in regions receiving too little [2,29]. The reason for poor homogeneous drug delivery is that these implants are solid and do not effectively fill the surgical cavity, especially in the case of the irregular shapes of the surgical cavity in GBM tumors. Chemotherapeutics currently used in GBM are limited only to drugs which cross the blood brain barrier.

In this study, we aimed to develop an injectable hydrogel delivery system which can completely fill the three-dimensional volume of the surgical cavity, deliver a homogeneous RT dose to all areas of the surgical cavity (including additional targeted margin) regardless of the shape of the cavity, and locally deliver chemotherapeutic agents. We have previously explored the use of biodegradable polymeric implants loaded with a radioisotope for localized radiotherapy using chitosan crosslinked with glutaraldehyde. These devices were biocompatible and biodegradable, however, these implants were solid (not injectable) and did not fill the entire surgical cavity [13,30,31]. We have fine-tuned the conditions for

Author Manuscript Author Manuscript Author Manuscript Author Manuscript

developing injectable chitosan biodegradable hydrogel implants by decreasing the previously published crosslinker concentration. Glutaraldehyde concentrations of 0.4% allowed for the best injectability properties. Injectability was described as the performance of the formulation during injection and takes into consideration the force required for injection, evenness of flow, and lack of clogging while injecting [14]. The injectability properties of chitosan hydrogels 0.4% (medium injection difficulty obtaining steady flow) were not affected by the incorporation of the alginate microcapsules.

We first wanted to demonstrate different release properties from the different compartments of the device by using the same probe. Therefore, as a proof of concept, we used one molecule that can be used in all compartments and provide a comparable detection properties (fluorescein), which will limit the variability of the results due to using different probes. Fluorescein was used once as a small molecule (FITC) directly dispersed in the hydrogel (not encapsulated), which demonstrated fast release; second as a large molecule (BSA-FITC) directly dispersed in the hydrogel (not encapsulated), which demonstrated slower release due to size; and third as a large molecule (BSA-FITC) encapsulated in the particles and then dispersed in the hydrogel which demonstrated the slowest release (Figure 4A).

We found that fluorescein as a free drug was released relatively fast from the hydrogel within the first few days. However, when conjugated to albumin the release was significantly reduced to about 50% over 42 days, this is probably because the pore distribution in the hydrogel solution, hinder the free diffusion of the high molecular weight BSA molecule. We hypothesized the conjugation to a large molecule will help slow the diffusion out of the hydrogel based on previous literature showing fast release of small drugs compared to slow release of high molecular weight BSA molecules from the same hydrogel delivery system [32]. When FITC was conjugated to albumin and encapsulated in alginate microparticles the release of fluorescein was completely blocked up to 42 days, probably also affected by the attractions between carboxyl groups (−COOH) on the alginate chain and the amine group ($-NH_2$) of BSA, as well as, the hydrogen bonds between the −COOH from alginate and −COOH from BSA, all restrict BSA release from the microparticle dispersed in the hydrogel [32].

After we proved this concept, we performed release experiments from the different compartments with the different therapeutic entities. We performed release of TMZ when it was directly dispersed into the hydrogel (Figure 4C), showing fast release. Simultaneously, we also aimed to keep the radioactive materials evenly distributed but trapped locally in the hydrogel preventing them from leaking out and distributing systemically. We developed two strategies to prevent the release of radioactivity from the hydrogel; the first was to conjugate the iodine radioisotope to a large molecule such as HSA, which was chosen due to its biocompatibility properties. Furthermore, we encapsulated the iodinated-HSA into crosslinked alginate microparticles, which is known to be biodegradable, biocompatible and to interact with chitosan [22,33–35], to further immobilize and prevent the release of the iodinated-HSA.

Author Manuscript Author Manuscript Author Manuscript Author Manuscript

We chose ^{131}I as radio therapeutic agent because it emits β particles with low penetrating properties (0.6 to 2.0 mm), which allows local radiotherapy at the site of implantation with minimal damage to distant tissues. Moreover, it was used due to its relatively short half-life (8 days) which will allow the decay of the isotope before it is released. In comparison, ^{125}I decays by electron capture to ^{125}Te followed by gamma-decay that can reach to distant tissues, with a half-life of 59.49 days[36]. If β emitters are found to be not an effective therapy for stem cell mediated resistance or inflammation-driven progression in gliomas, a more potent α emitters could be tested, but their efficacy in large distances should be carefully considered [37]. The in vitro studies were performed at 42 days because it is about 5 half-lives of ^{131}I, which is the time point where the radioactive dose will be less than 5% (3.125%) of the original dose of ^{131}I, and the resulting stable isotope ^{131}Xe and residual iodine will be considered not radioactive anymore. This way we could confirm that the device will allow the decay of ^{131}I the while it is still encapsulated in the hydrogel to promote local radiotherapy. We found that the release of ^{131}I was negligible over 42 days, while the TMZ was completely released over the first 48 hours. Here, we describe a novel delivery system that is injectable and allows tunable release profiles of different molecules to release chemotherapy locally while retaining radiotherapy to promote localized therapy.

We then tested the release properties of the chemotherapy and radiotherapy from the hydrogel *in vivo*. First, we tested the biodistribution of albumin-conjugated ^{131}I to different organs when encapsulated in alginate microparticles and introduced into the hydrogel, and the hydrogels were locally transplanted onto a tumor. We found that radioactivity was completely retained in the tumor bed with negligible distribution to other tissues. Moreover, we compared the biodistribution of chemotherapy when directly dispersed in the hydrogel and delivered locally as a hydrogel implant, to the systemic delivery in the form of an intravenous injection. We found that when delivered locally the chemotherapy accumulated in the tumor at 10-fold higher concentrations compared to when delivered systemically. Moreover, we found that the biodistribution of the chemotherapy to other organs following local delivery was lower than when delivered systemically.

Finally, we determined the therapeutic efficacy of the hydrogel for local delivery of chemo or radiotherapy. Hydrogels loaded with chemotherapy or radiotherapy were implanted on GBM tumors. The survival and tumor progression in these animals were compared to animals implanted with empty hydrogel controls. Tumors were significantly decreased and survival was improved in both treatments groups compared to the control group. In future studies, orthotopic brain tumor models in small animals (mice)[38,39] and big animals (dogs)[40,41] will be evaluated for therapeutic efficacy of the hydrogel for local delivery of chemo or radiotherapy after brain surgery. The effective treatments will depend on experimental models that closely resemble human GBM characteristics for testing injectability and toxicity and providing an accurate model for efficacy testing. Murine models of GBM appear to recapitulate several of the human GBM histopathological features and, considering their reproducibility and availability, they constitute a valuable in vivo system for preclinical studies. However, dog GBMs models exhibited endothelial proliferation, a key feature that is absent in murine models, as well as, presented a spontaneous tumor in the context of a larger brain [41].

Author Manuscript Author Manuscript Author Manuscript Author Manuscript

On one hand, implantation of iodine-125 seeds allowed the dose distribution to be determined pre- and post-operatively, however, inhomogeneous dose distribution in the surgical cavity after may lead to radionecrosis in the overdosed areas and recurrence in the underdosed regions [29,42,43]. On the other hand, the balloon system (GliaSite) delivers a more conformal, uniform and relatively homogeneous dose distribution [44], but due to its fixed dosimetric geometry some concerns still arise [2]. Therefore, compared to traditional localized treatment, the local treatment conducted with a novel, injectable and biodegradable implant provides a highly efficacious therapy with decreased side effects in distant organs as well as to the normal tissues surrounding the tumor bed. Another substantial advantage of this system is that it allows the use of different therapeutic agents with different sizes and different chemical properties irrespective of their ability to cross the blood-brain barrier including small molecules and large molecules. This innovative strategy opens a new window for a wide array of novel therapies which do not cross the blood-brain barrier (i.e antibodies) and may now potentially be tested in the treatment of brain tumors. The data discussed herein provide the preclinical basis for future trials to test the effect of the chemo-radio-hydrogel implants to improve the local control of glioma and other brain tumors. Furthermore, this technology can be further used for other tumor types that can be surgically removed and require treatment of the tumor bed. In conclusion, the development of novel injectable biodegradable chemo-radio-hydrogel implants may potentially improve the local control and overall outcome of aggressive, poor prognosis brain tumors as well as other locally, aggressive resectable tumors.

Supplementary Material

Refer to Web version on PubMed Central for supplementary material.

ACKNOWLEDGEMENTS

We want to thank Sanmathi Chavalmane from the Nano Research Facility (NRF), School of Engineering and Applied Science at Washington University in St. Louis, for her help with FTIR analysis and interpretation. Abdel Kareem Azab is supported by grants from National Institutes of Health under Award Number U54CA199092, the Multiple Myeloma Research Foundation, the International Waldenstrom Macroglobulinemia Foundation and Bear Cub Award (Skandalaris Center at Washington University in St. Louis).

REFERENCES

1. Kreth FW , Thon N , Siefert A , Tonn JC 2010 The place of interstitial brachytherapy and radiosurgery for low-grade gliomas. Advances and technical standards in neurosurgery 35:183–212. [PubMed: 20102115]
2. de la Puente P , Azab AK 2014 Delivery systems for brachytherapy. J Control Release 192:19–28. [PubMed: 25008970]
3. Chino K , Silvain D , Grace A , Stubbs J , Stea B 2008 Feasibility and safety of outpatient brachytherapy in 37 patients with brain tumors using the GliaSite Radiation Therapy System. Medical physics 35(7):3383–3388. [PubMed: 18697562]
4. Mundinger F , Ostertag CB , Birg W , Weigel K 1980 Stereotactic treatment of brain lesions. Biopsy, interstitial radiotherapy (iridium-192 and iodine-125) and drainage procedures. Applied neurophysiology 43(3–5):198–204. [PubMed: 7027939]
5. Mundinger F , Braus DF , Krauss JK , Birg W 1991 Long-term outcome of 89 low-grade brain-stem gliomas after interstitial radiation therapy. Journal of neurosurgery 75(5):740–746. [PubMed: 1919696]

Author Manuscript Author Manuscript Author Manuscript Author Manuscript

6. Scharfen CO , Sneed PK , Wara WM , Larson DA , Phillips TL , Prados MD , Weaver KA , Malec M , Acord P , Lamborn KR , et al. 1992 High activity iodine-125 interstitial implant for gliomas. International journal of radiation oncology, biology, physics 24(4):583–591.
7. Johannesen TB , Watne K , Lote K , Norum J , Hennig R , Tvera K , Hirschberg H 1999 Intracavity fractionated balloon brachytherapy in glioblastoma. Acta Neurochir 141(2):127–133. [PubMed: 10189493]
8. Dempsey JF , Williams JA , Stubbs JB , Patrick TJ , Williamson JF 1998 Dosimetric properties of a novel brachytherapy balloon applicator for the treatment of malignant brain-tumor resection-cavity margins. International journal of radiation oncology, biology, physics 42(2):421–429.
9. Selker RG , Shapiro WR , Burger P , Blackwood MS , Arena VC , Gilder JC , Malkin MG , Mealey JJ ., Neal JH , Olson J , Robertson JT , Barnett GH , Bloomfield S , Albright R , Hochberg FH , Hiesiger E , Green S , Brain Tumor Cooperative G 2002 The Brain Tumor Cooperative Group NIH Trial 87–01: a randomized comparison of surgery, external radiotherapy, and carmustine versus surgery, interstitial radiotherapy boost, external radiation therapy, and carmustine. Neurosurgery 51(2):343–355; discussion 355–347. [PubMed: 12182772]
10. Giese A , Kucinski T , Knopp U , Goldbrunner R , Hamel W , Mehdorn HM , Tonn JC , Hilt D , Westphal M 2004 Pattern of recurrence following local chemotherapy with biodegradable carmustine (BCNU) implants in patients with glioblastoma. J Neurooncol 66(3):351–360. [PubMed: 15015668]
11. Zhang YD , Dai RY , Chen Z , Zhang YH , He XZ , Zhou J 2014 Efficacy and safety of carmustine wafers in the treatment of glioblastoma multiforme: a systematic review. Turk Neurosurg 24(5): 639–645. [PubMed: 25269031]
12. Carlson BL , Pokorny JL , Schroeder MA , Sarkaria JN 2011 Establishment, maintenance and in vitro and in vivo applications of primary human glioblastoma multiforme (GBM) xenograft models for translational biology studies and drug discovery. Curr Protoc Pharmacol 14(14).
13. Azab AK , Orkin B , Doviner V , Nissan A , Klein M , Srebnik M , Rubinstein A 2006 Crosslinked chitosan implants as potential degradable devices for brachytherapy: in vitro and in vivo analysis. Journal of controlled release : official journal of the Controlled Release Society 111(3):281–289. [PubMed: 16499987]
14. Cilurzo F , Selmin F , Minghetti P , Adami M , Bertoni E , Lauria S , Montanari L 2011 Injectability Evaluation: An Open Issue. AAPS Pharm Sci Tech 12(2):604–609.
15. Reddy K , Damek D , Gaspar LE , Ney D , Waziri A , Lillehei K , Stuhr K , Kavanagh BD , Chen C 2012 Phase II trial of hypofractionated IMRT with temozolomide for patients with newly diagnosed glioblastoma multiforme. Int J Radiat Oncol Biol Phys 84(3):655–660. [PubMed: 22483738]
16. Howell RW , Rao DV , Sastry KS 1989 Macroscopic dosimetry for radioimmunotherapy: nonuniform activity distributions in solid tumors. Medical physics 16(1):66–74. [PubMed: 2921982]
17. Caro CA , Lillo L , Valenzuela FJ , Cabello G 2017 Mechanistic characterization and inhibition of sphingomyelinase C over substituted Iron Schiff bases of chitosan adsorbed on glassy carbon electrode. Chemico-biological interactions 263:81–87. [PubMed: 28038894]
18. Veit P , Forster C , Heinze K 2016 On the mechanism of imine elimination from Fischer tungsten carbene complexes. Beilstein journal of organic chemistry 12:1322–1333. [PubMed: 27559381]
19. Migneault I , Dartiguenave C , Bertrand MJ , Waldron KC 2004 Glutaraldehyde: behavior in aqueous solution, reaction with proteins, and application to enzyme crosslinking. BioTechniques 37(5):790–796, 798–802. [PubMed: 15560135]
20. Kumbar SG , Kulkarni AR , Aminabhavi M 2002 Crosslinked chitosan microspheres for encapsulation of diclofenac sodium: effect of crosslinking agent. Journal of microencapsulation 19(2):173–180. [PubMed: 11837972]
21. Ritschel WS K 1979 In vitro testing of injectability. Pharm Ind 41(5):468–474.
22. Braccini I , Perez S 2001 Molecular basis of C(2+)-induced gelation in alginates and pectins: the egg-box model revisited. Biomacromolecules 2(4):1089–1096. [PubMed: 11777378]
23. Schwartzbaum JA , Fisher JL , Aldape KD , Wrensch M 2006 Epidemiology and molecular pathology of glioma. Nature clinical practice Neurology 2(9):494–503; quiz 491 p following 516.

Author Manuscript Author Manuscript Author Manuscript Author Manuscript

24. Weller M , Cloughesy T , Perry JR , Wick W 2012 Standards of care for treatment of recurrent glioblastoma—are we there yet? Neuro-Oncology.

25. Hochberg FH , Pruitt A 1980 Assumptions in the radiotherapy of glioblastoma. Neurology 30(9): 907–911. [PubMed: 6252514]

26. Bashir R , Hochberg F , Oot R 1988 Regrowth patterns of glioblastoma multiforme related to planning of interstitial brachytherapy radiation fields. Neurosurgery 23(1):27–30. [PubMed: 2845294]

27. Stupp R , Hegi ME , Mason WP , van den Bent MJ , Taphoorn MJB , Janzer RC , Ludwin SK , Allgeier A , Fisher B , Belanger K , Hau P , Brandes AA , Gijtenbeek J , Marosi C , Vecht CJ , Mokhtari K , Wesseling P , Villa S , Eisenhauer E , Gorlia T , Weller M , Lacombe D , Cairncross JG , Mirimanoff R-O 2009 Effects of radiotherapy with concomitant and adjuvant temozolomide versus radiotherapy alone on survival in glioblastoma in a randomised phase III study: 5-year analysis of the EORTC-NCIC trial. The Lancet Oncology 10(5):459–466. [PubMed: 19269895]

28. Stupp R , Mason WP , van den Bent MJ , Weller M , Fisher B , Taphoorn MJB , Belanger K , Brandes AA , Marosi C , Bogdahn U , Curschmann J , Janzer RC , Ludwin SK , Gorlia T , Allgeier A , Lacombe D , Cairncross JG , Eisenhauer E , Mirimanoff RO 2005 Radiotherapy plus Concomitant and Adjuvant Temozolomide for Glioblastoma. New England Journal of Medicine 352(10):987–996. [PubMed: 15758009]

29. Larson DA , Suplica JM , Chang SM , Lamborn KR , McDermott MW , Sneed PK , Prados MD , Wara WM , Nicholas MK , Berger MS 2004 Permanent iodine 125 brachytherapy in patients with progressive or recurrent glioblastoma multiforme. Neuro-oncology 6(2):119–126. [PubMed: 15134626]

30. Azab AK , Doviner V , Orkin B , Kleinstern J , Srebnik M , Nissan A , Rubinstein A 2007 Biocompatibility evaluation of crosslinked chitosan hydrogels after subcutaneous and intraperitoneal implantation in the rat. Journal of biomedical materials research Part A 83(2):414–422. [PubMed: 17455216]

31. Azab AK , Kleinstern J , Doviner V , Orkin B , Srebnik M , Nissan A , Rubinstein A 2007 Prevention of tumor recurrence and distant metastasis formation in a breast cancer mouse model by biodegradable implant of 131I-norcholesterol. Journal of controlled release : official journal of the Controlled Release Society 123(2):116–122. [PubMed: 17854940]

32. Zhao J , Zhao X , Guo B , Ma PX 2014 Multifunctional interpenetrating polymer network hydrogels based on methacrylated alginate for the delivery of small molecule drugs and sustained release of protein. Biomacromolecules 15(9):3246–3252. [PubMed: 25102223]

33. Finotelli PV , Da Silva D , Sola-Penna M , Rossi AM , Farina M , Andrade LR , Takeuchi AY , Rocha-Leao MH 2010 Microcapsules of alginate/chitosan containing magnetic nanoparticles for controlled release of insulin. Colloids Surf B Biointerfaces 81(1):206–211. [PubMed: 20688491]

34. Tonnesen HH , Karlsen J 2002 Alginate in drug delivery systems. Drug Dev Ind Pharm 28(6):621–630. [PubMed: 12149954]

35. Sosnik A 2014 Alginate Particles as Platform for Drug Delivery by the Oral Route: State-of-the-Art. ISRN Pharm 9(926157).

36. Narra VR , Howell RW , Harapanhalli RS , Sastry KS , Rao DV 1992 Radiotoxicity of some iodine-123, iodine-125 and iodine-131-labeled compounds in mouse testes: implications for radiopharmaceutical design. Journal of nuclear medicine : official publication, Society of Nuclear Medicine 33(12):2196–2201.

37. Sofou S 2008 Radionuclide carriers for targeting of cancer. International Journal of Nanomedicine 3(2):181–199. [PubMed: 18686778]

38. Martinez-Murillo R , Martinez A 2007 Standardization of an orthotopic mouse brain tumor model following transplantation of CT-2A astrocytoma cells. Histology and histopathology 22(12):1309–1326. [PubMed: 17701911]

39. Kramp TR , Camphausen K 2012 Combination Radiotherapy in an Orthotopic Mouse Brain Tumor Model. Journal of Visualized Experiments : JoVE (61):3397. [PubMed: 22415465]

40. Dickinson PJ , LeCouteur RA , Higgins RJ , Bringas JR , Larson RF , Yamashita Y , Krauze MT , Forsayeth J , Noble CO , Drummond DC , Kirpotin DB , Park JW , Berger MS , Bankiewicz KS

Author Manuscript Author Manuscript Author Manuscript Author Manuscript

2010 Canine spontaneous glioma: A translational model system for convection-enhanced delivery. Neuro-Oncology 12(9):928–940. [PubMed: 20488958]

41. Candolfi M , Curtin JF , Stephen Nichols W , Muhammad AG , King GD , Elizabeth Pluhar G , McNiel EA , Ohlfest JR , Freese AB , Moore PF , Lerner J , Lowenstein PR , Castro MG 2007 Intracranial glioblastoma models in preclinical neuro-oncology: neuropathological characterization and tumor progression. Journal of neuro-oncology 85(2):133–148. [PubMed: 17874037]
42. Wowra B , Schmitt HP , Sturm V 1989 Incidence of late radiation necrosis with transient mass effect after interstitial low dose rate radiotherapy for cerebral gliomas. Acta neurochirurgica 99(3–4):104–108. [PubMed: 2549766]
43. Andrews DW , Scott CB , Sperduto PW , Flanders AE , Gaspar LE , Schell MC , Werner-Wasik M , Demas W , Ryu J , Bahary JP , Souhami L , Rotman M , Mehta MP , Curran WJ 2004 Whole brain radiation therapy with or without stereotactic radiosurgery boost for patients with one to three brain metastases: phase III results of the RTOG 9508 randomised trial. Lancet 363(9422): 1665–1672. [PubMed: 15158627]
44. Ling CC , Anderson LL , Shipley WU 1979 Dose inhomogeneity in interstitial implants using 125I seeds. International journal of radiation oncology, biology, physics 5(3):419–425.

Author Manuscript
Author Manuscript
Author Manuscript
Author Manuscript

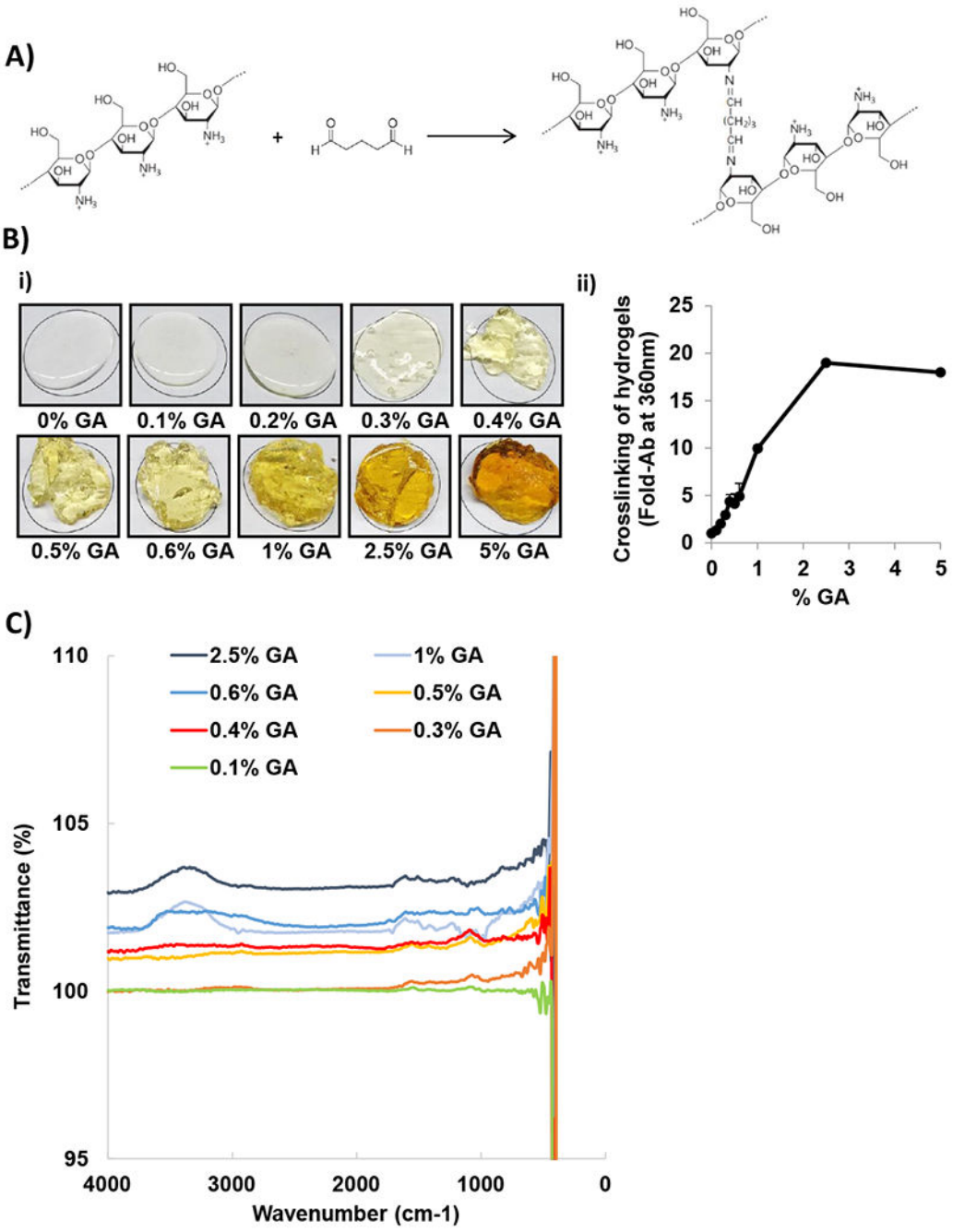

Figure 1: Chemical characterization of crosslinked chitosan hydrogels

A) Chemical structure of chitosan, glutaraldehyde (GA), and crosslinking reaction showing the nucleophilic attack of the amine group of the chitosan to the positively charged aldehyde group of GA forming an imine group in the chitosan hydrogels crosslinked with GA. (ChemDraw Professional 15.1 was used for the chemical drawings). **B)** Physical appearance of chitosan hydrogels crosslinked with increasing GA concentrations **i)** 0%, 0.1%, 0.2%, 0.3%, 0.4%, 0.5%, 0.6%, 1%, 2.5%, and 5%; **ii)** quantification of crosslinking based on GA

concentrations measured by the absorption of the hydrogels at 360 nm (n=3). **C)** FTIR spectra of crosslinking based on GA concentrations.

Author Manuscript Author Manuscript Author Manuscript Author Manuscript

Author Manuscript Author Manuscript Author Manuscript Author Manuscript

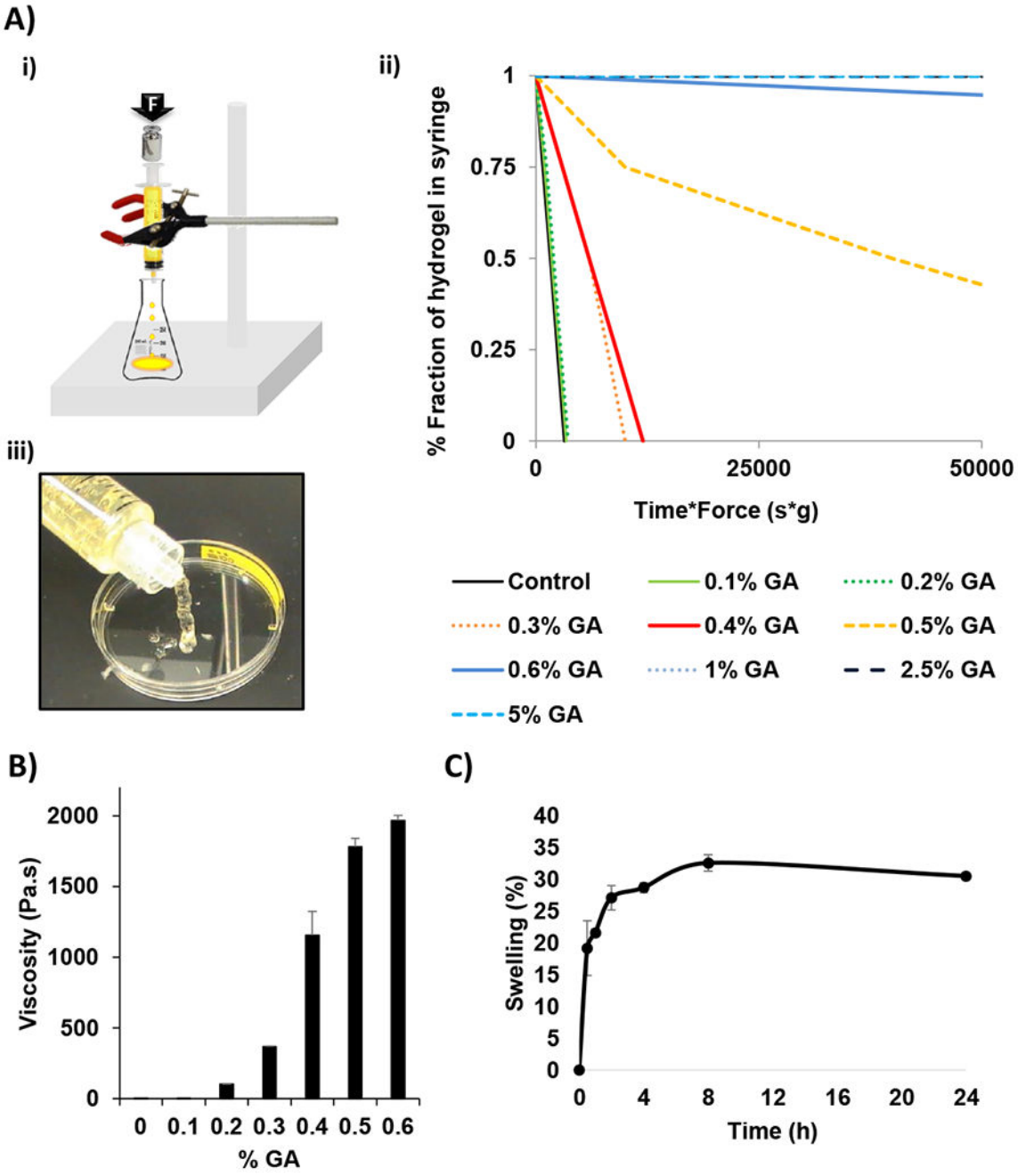

Figure 2: Characterization of viscosity, injectability and swelling of crosslinked chitosan hydrogels

A) i) Design of machine used to determine the injectable properties where a constant mass is applied on top of a filled syringe and the time required to release the fractions of hydrogel from the syringe is measured. **ii)** The injectability of the chitosan hydrogels crosslinked with increasing GA concentrations represented as the fraction of the hydrogel in the syringe in function of the shear force*time needed for emptying the syringe (n=3), and **iii)** image of the injectability properties of chitosan hydrogel crosslinked with 0.4% GA as an example of the

Author Manuscript Author Manuscript Author Manuscript Author Manuscript

best injectability properties. **B)** Viscosity measurements of chitosan crosslinked hydrogels with increasing GA concentration (n=3). **C)** Swelling kinetics of chitosan hydrogels crosslinked with 0.4% GA in DDW (n=3).

Author Manuscript Author Manuscript Author Manuscript Author Manuscript

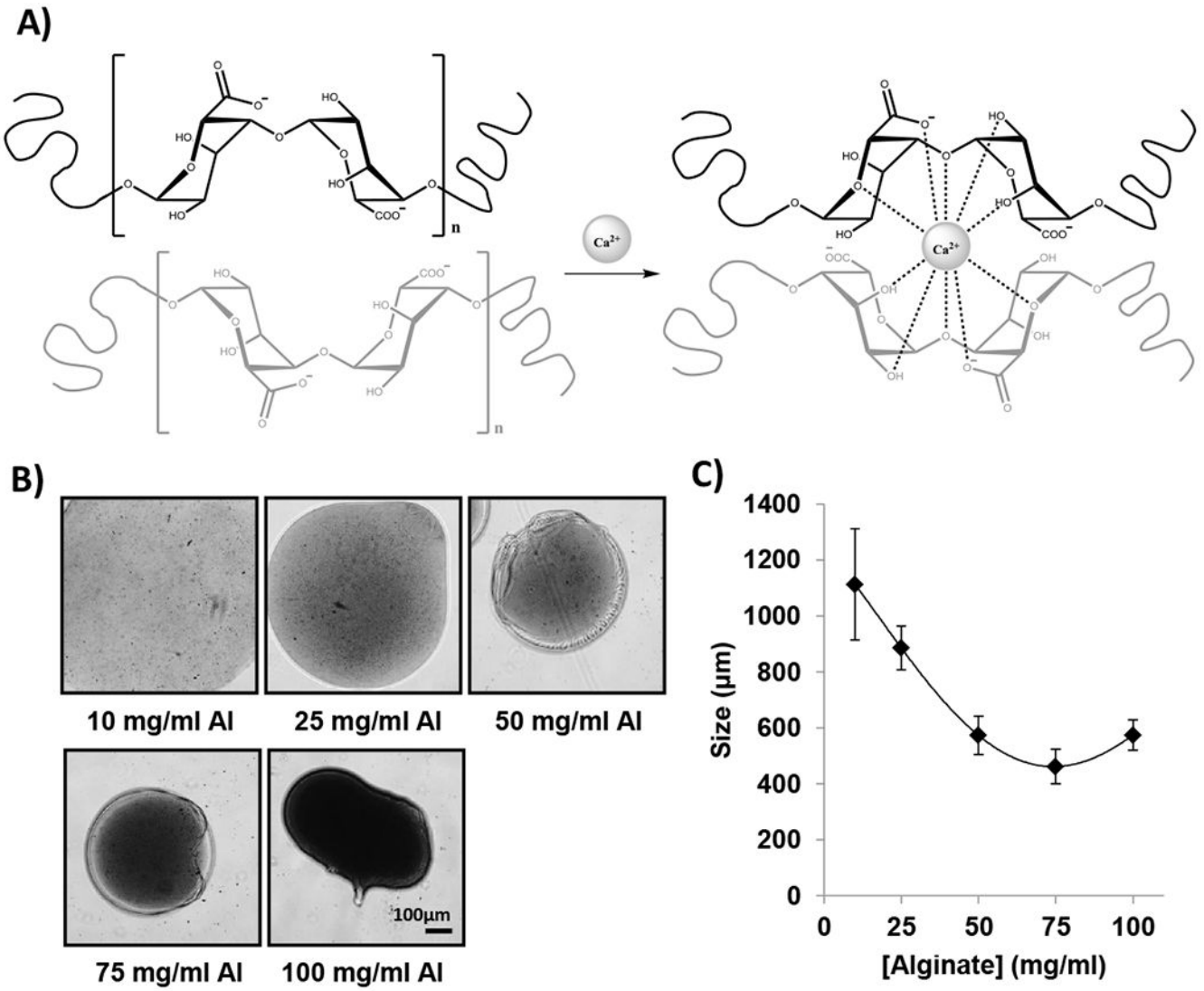

Figure 3: Characterization of alginate microparticles

A) Chemical structure of alginate, calcium ions (Ca^{2+}), and crosslinking reaction showing the interaction of positive calcium ions (+2) with the carboxylic acid groups of two alginate chains (upper chain in black and lower chain in light gray) in the crosslinked alginate microparticles forming an egg-box structure. (ChemDraw Professional 15.1 was used for the chemical drawings). **B)** Representative images of the morphology of alginate particles crosslinked with $CaCl_2$ 0.1M using different alginate concentration: 10 mg/ml, 25 mg/ml, 50 mg/ml, 75 mg/ml, and 100 mg/ml. Scale Bar: 100µm. **C)** Effect of alginate concentration (10 – 100 mg/ml) in microparticles size (n=10).

Author Manuscript Author Manuscript Author Manuscript Author Manuscript

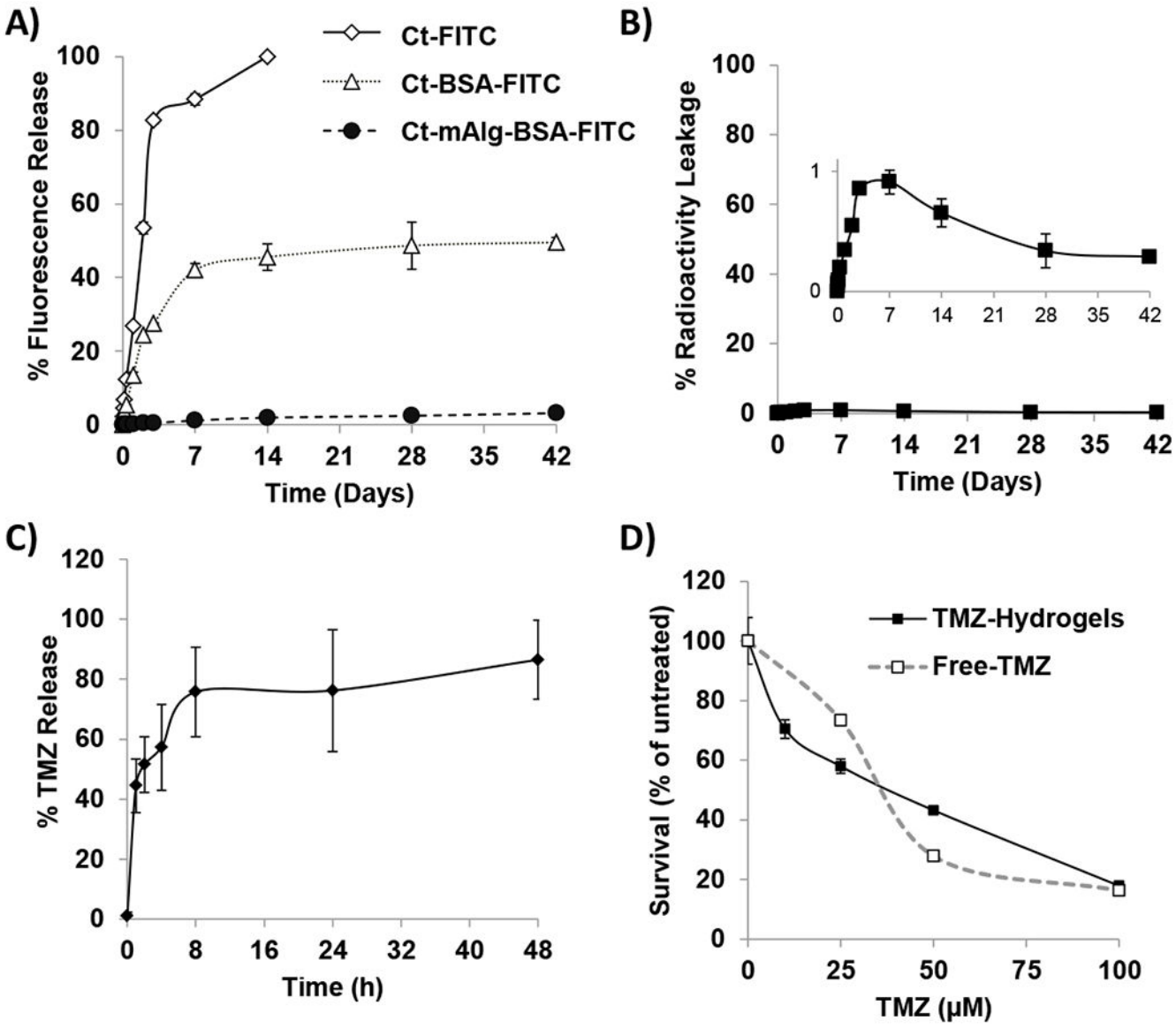

Figure 4: *In vitro* studies of chemo- radiotherapy

A) Release profile of fluorescence from chitosan hydrogels loaded with free FITC or BSA-FITC, and BSA-FITC encapsulated in alginate microparticles (mAlg) and incorporated in chitosan hydrogels for 42 days (n=3). **B)** Percent of radioactive leakage of ^{131}I-HSA out of 75mg/ml alginate microparticles loaded inside ct hydrogels for 42 days (n=3). Note insert that shows minimal (less than 1%) radioactive leakage. **C)** Drug release profile from chitosan hydrogels loaded with temozolomide (TMZ) for 48 hours (n=3). **D)** The effect of TMZ concentrations (0 – 100 μM) of free-drug or TMZ-hydrogels for three days on the survival of D54 cells analyzed by MTT (n=3).

Author Manuscript Author Manuscript Author Manuscript Author Manuscript

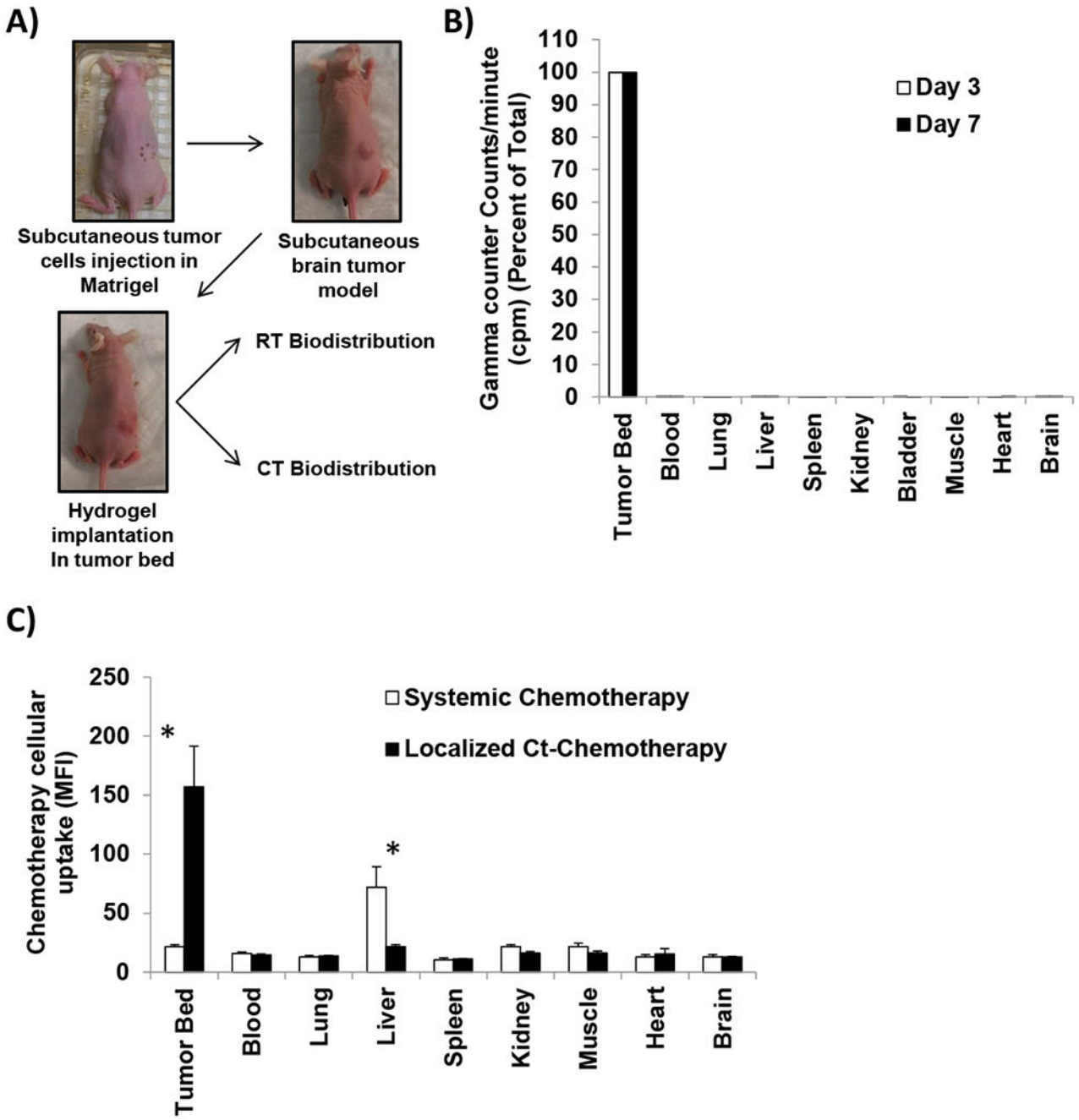

Figure 5: *In vivo* studies of localized chemo- radiotherapy

A) Design of *in vivo* subcutaneous brain tumor model, in which D54 GBM cells are injected in combination with matrigel, once tumors were palpable, mice were stratified into treatment groups where Ct hydrogels were implanted on top of the tumors and mice were followed by BLI twice a week, analyzed for radiotherapy and chemotherapy release. **B)** Radiotherapy bio-distribution in different organs after 3 and 7 days of implantation of radio-hydrogels measured by gamma counter (counts per minute, cpm) (n=3). **C)** Chemotherapy cellular uptake in different organs after 18 hours of implantation of localized chemo-hydrogels

loaded with doxorubicin or i.v. systemic injection of same amount of doxorubicin (5mg/kg) measured by MFI in flow cytometry (n=3).

Author Manuscript Author Manuscript Author Manuscript Author Manuscript

Author Manuscript Author Manuscript Author Manuscript Author Manuscript

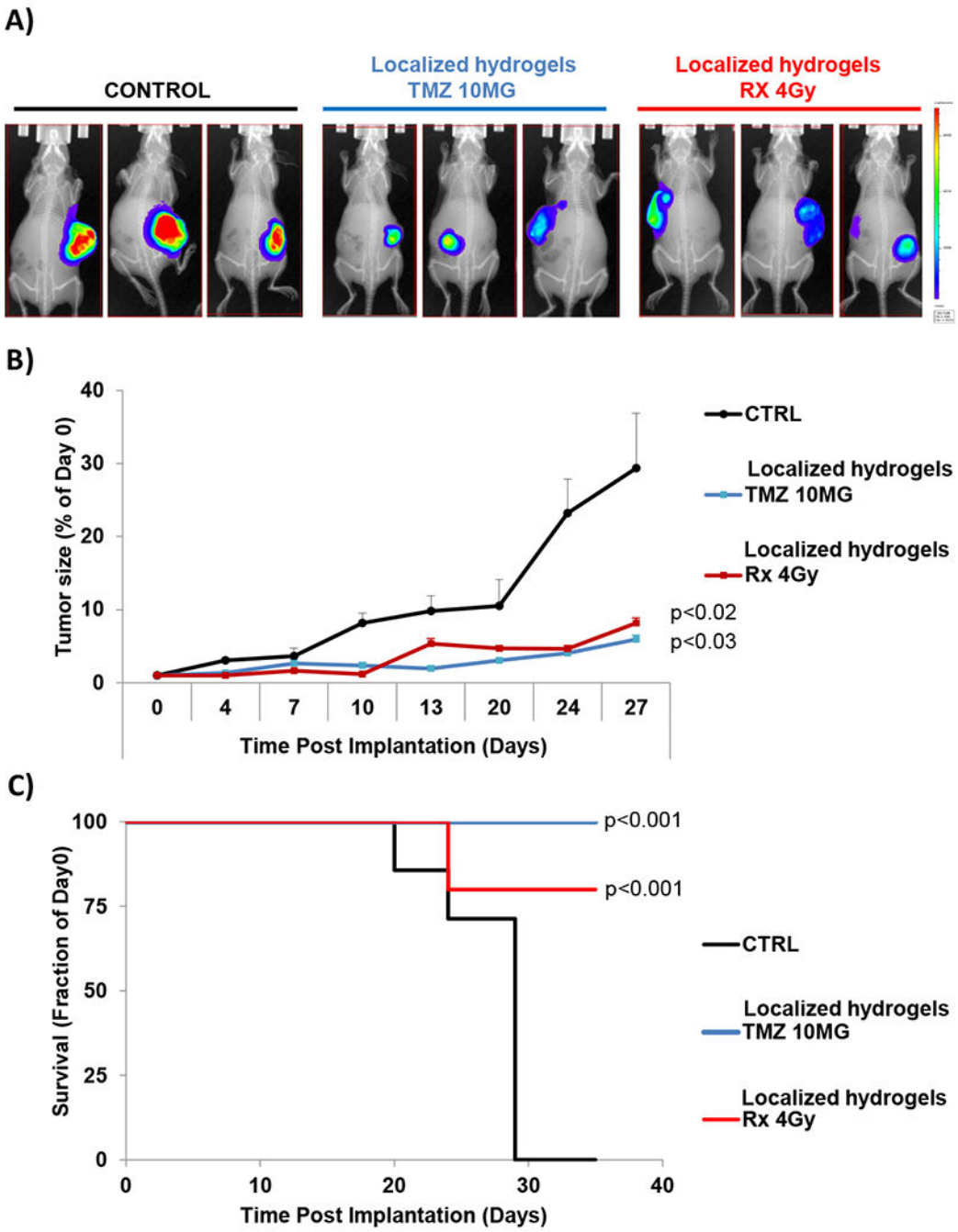

Figure 6: Localized chemo- or radio-therapy hydrogels improves survival by inhibiting tumor growth.

Nude mice were implanted subcutaneously with D54 cells stably expressing luciferase mixed with matrigel. After 10 days, mice were imaged with bioluminescence imaging and then stratified into three groups of ten mice each. Mice were treated with localized TMZ-hydrogels (10mg) or ^{131}I-hydrogels (4Gy) or controlled empty hydrogel. **A)** Representative BLI pictures of three mice implanted with control (left), chemotherapy (middle) or radiotherapy hydrogels (right) at day 27 after implantation. **B)** The effect of hydrogel

implantation (empty-control, TMZ, or Rx-4Gy) on tumor progression monitored for 27 days using bioluminescent imagining (BLI) and shown as the average of the luminescent signal of ten mice. **C)** Kaplan-Meyer survival curves following various treatments of mice bearing subcutaneous brain tumors.

Author Manuscript Author Manuscript Author Manuscript Author Manuscript

Author Manuscript

Author Manuscript

Author Manuscript

Author Manuscript

Table 1:

Score of manual injectability of chitosan hydrogels crosslinked with 0 – 5% glutaraldehyde. Injectability of syringe filled with aliquots of 4 ml of each formulation was considered acceptable when the total score was up to 30 ± 2, meaning they were able to inject the tested formulation with medium difficulty obtaining steady flow.

Chitosan hydrogels (% of Glutaraldehyde)	*Individuals Score*										*Total Score*
	#1	**#2**	**#3**	**#4**	**#5**	**#6**	**#7**	**#8**	**#9**	**#10**	
Control	4	4	4	4	4	4	4	4	4	4	40
0.1%	4	4	4	4	4	4	4	4	4	4	40
0.2%	4	4	4	4	4	4	4	4	4	4	40
0.3%	3	4	4	3	3	3	4	4	3	3	34
0.4%	3	3	3	3	3	3	3	3	3	3	30
0.5%	2	2	2	3	2	3	2	2	2	2	22
0.6%	1	1	1	1	1	1	1	1	1	1	10
1%	1	1	1	1	1	1	1	1	1	1	10
2.5%	1	1	1	1	1	1	1	1	1	1	10
5%	1	1	1	1	1	1	1	1	1	1	10